



Room temperature ferromagnetism in Mn doped ZnO: Co nanoparticles by co-precipitation method

V. Pazhanivelu^a, A. Paul Blessington Selvadurai^a, Yongsheng Zhao^b, R. Thiyagarajan^b, R. Murugaraj^{a,*}

^a Department of Physics, Anna University, Chennai 600044, India

^b Center for High Pressure Science and Technology Advanced Research, 1690 Cailun Road, Shanghai 201203, China

ARTICLE INFO

Article history:

Received 19 September 2015

Received in revised form

20 October 2015

Accepted 23 October 2015

Available online 28 October 2015

Keywords:

Doped ZnO

Nanoparticles

Photoluminescence

Electron paramagnetic resonance

Zn interstitial defects

RTFM

ABSTRACT

In this present work, the Mn^{2+} and Co^{2+} ions doping and co-doping effect on the structural, vibrational, morphological, optical and magnetic behaviors of ZnO based dilute magnetic semiconductors are reported. The $Zn_{0.95}Co_{0.05}O$ (ZC), $Zn_{0.95}Mn_{0.05}O$ (ZM) and $Zn_{0.90}Co_{0.05}Mn_{0.05}O$ (ZCM) samples were prepared by co-precipitation method. From the XRD analysis, it was observed that on the doping of Mn^{2+} ion in ZnO matrix, decreases their crystalline nature as well as the crystallite size significantly. The Raman spectra, Photoluminescence and electron paramagnetic resonance spectroscopy measurements reveal that the presence of defects in prepared samples. The UV-DRS spectroscopic exhibits the incorporation of dopant ions and their effect on the band gap subsequently. The magnetization measurements suggest the room temperature ferromagnetism (RTFM) in the prepared samples. The observed RTFM phenomenon was discussed based on the defects and grain confinement.

© 2015 Elsevier B.V. All rights reserved.

1. Introduction

Dilute Magnetic Semiconductors (DMSs) have attracted great interest in the recent years, because of their state-of-the-art applications in the field of modern information technology through the spintronic devices. Also, they have been widely used in multifunctional fields such as optical, optoelectronic, varistor and gas sensing, etc. [1]. In particular, ZnO is one of the prototypical metal oxide semiconductors having a wide band gap (3.327 eV) and large exciton binding energy (60 meV). Generally, one may expect that the perturbations such as impurity doping and/or sintering can change the basic characteristics of the physical systems through by altering their electronic configurations. In ZnO based DMS materials, a low concentration impurity doping and sintering environment also affects its physical properties. Earlier, Dietl et al., reported that the existence of RTFM with a *p*-type semiconducting properties in Mn-doped ZnO system [2]. However, the doping of other transition-metal (TM) ions such as Cr [3], Mn [4,5], Fe [6], Ni [7], Co [8–10] and Cu [11] also shows RTFM behavior irrespective of physical forms such as powders and/or thin films. Particularly, the co-doping of Alkali [12], Alkaline metal ions [13] and rare-earth ions (RE) [14] with TM: ZnO powders have

been widely studied both theoretically and experimentally by various research groups around the world.

So far, various preparation methods such as sputtering, spray-pyrolysis, Metal–Organic Chemical Vapor Deposition (MOCVD) and Pulsed Laser Deposition (PLD) were reported for co-doping of Mn ions in doped ZnO thin films [15–24]. Apart from thin film formations, there were some reports on bulk form of Mn codoped ZnO:Co nanomaterials with different reasoning for the presence of RTFM. Out of them, a few reports are as follows: The Li^+ co-doped and Li^{3+} ions irradiate ZnO:Mn powders prepared by co-precipitation and solid state reaction method, respectively. Both the systems exhibit RTFM due to their Zn vacancy defects [25,26]. However, the Mn codoped with Fe and Cr ions prepared by solid state reaction and hydrothermal method respectively, explained the RTFM behavior through bounded magnetic polarons (BMP) exchange interactions [27,28]. Kai-Cheng Zhang et al., theoretically predicted that the suppression of the AFM exchange interaction and enhancement of RTFM in ZnO:Mn system through the hole-mediated double-exchange interactions [29]. But, Duan et al., prepared Mn–Co codoped ZnO powders by auto-combustion method and the presence of lattice defects is a reason for RTFM in this system [30].

Similarly, Hengda Li et al., reported that the doping concentration of Mn plays a crucial role in RTFM of Mn co-doped ZnO: Co nanoparticles prepared by the sol–gel method. According to the

* Corresponding author.

E-mail address: r.murugaraj@gmail.com (R. Murugaraj).

RKKY theory, the doping concentration of Mn increases the delocalized carrier concentrations in the sample. Subsequently, the exchange interactions between the delocalized carriers and the conduction band electrons were led to RTFM behavior [31]. Sabiu et al., reported that $\text{Zn}_{0.9-x}\text{Co}_{0.1}\text{Mn}_x\text{O}$ exhibits RTFM by lattice defects such as Zn interstitial and O vacancies upto $x=0.2$ [32]. According to previous reports, the different preparation methods for TM doped ZnO nanomaterials and suggested the various phenomena for the existence of RTFM. In general, the doping element induces the lattice defects and alters the carrier concentrations in the ZnO doped sample. Till now, the mechanism behind RTFM was claimed by exchange interactions such as double-exchange, super-exchange and dopant electrons-delocalized conduction band electron interactions. The dopant related secondary phase formations, magnetic clusters and metal precipitations were played a vital role in the magnetic behavior of doped ZnO systems. Hence, the origin of RTFM is still not completely relieved, and open up a new window in spintronics materials research.

By keeping these points in mind, we aim to investigate the doping effect of Co, Mn and co-doping of Co, Mn ions in ZnO nanoparticles through standardized procedures. Even though there are so many reports on the same compositions, we do again the same for comparing our results with different sample forms and preparation techniques.

2. Experimental

The $\text{Zn}_{0.95}\text{Co}_{0.05}\text{O}$ (ZC), $\text{Zn}_{0.95}\text{Mn}_{0.05}\text{O}$ (ZM) and $\text{Zn}_{0.90}\text{Co}_{0.05}\text{Mn}_{0.05}\text{O}$ (ZCM) nanoparticle samples were prepared by co-precipitation method with precursors such as zinc acetate [$\text{Zn}(\text{CH}_3\text{COO})_2 \cdot \text{H}_2\text{O}$], cobalt acetate [$\text{Co}(\text{CH}_3\text{COO})_2 \cdot 4\text{H}_2\text{O}$], [Mn ($\text{CH}_3\text{COO})_2 \cdot 4\text{H}_2\text{O}$] and oxalic acid [$(\text{COOH})_2 \cdot 2\text{H}_2\text{O}$] as starting materials [10]. The crystalline nature of the samples was confirmed by the powder XRD patterns using Bruker D2 Phaser X-Ray Diffractometer. The surface morphology was characterized by Scanning Electronic Microscopy (SEM; FEI Quanta FEG 200 model). The Raman scattering spectral measurements were carried out for the prepared samples using Renishaw inVia Reflex system with 0.6 mW power of Ar^+ ion laser with excitation wavelength of 488 nm at room temperature. The UV Diffuse Reflectance Spectroscopy (DRS) (Shimadzu UV 2450 PC spectrophotometer) and Photoluminescence (JY Fluorolog-3 spectrofluorometer) studies was carried out to investigate the optical and emission properties of the samples respectively. The EPR measurements were performed on a JEOL-JES FA200 spectrometer at room temperature on powdered samples. The magnetic property of all the samples at room temperature was analyzed through the magnetic field dependence of magnetization measurements using Lakeshore-7404 vibrating sample magnetometer.

3. Results

3.1. Structural properties

The powder XRD pattern for all the samples have been employed with $\text{Cu-K}\alpha$ ($\lambda=1.542 \text{ \AA}$) radiation at a constant slow scanning rate of 0.20 s^{-1} and are shown in Fig. 1(a). The observed XRD patterns confirmed that all compositions are found to be in a single phase. They are also in good agreement with the standard pattern of pure ZnO [JCPDS no. 76-0704] at room temperature and belonging to the hexagonal Wurtzite structure. Compared with ZC sample, the peak positions of XRD patterns for doped compounds such as ZM and ZCM shifts towards the higher angle slightly. However, the intensity of the diffraction peaks is decreased appreciably. This is attributed due to the decreasing of the grain size

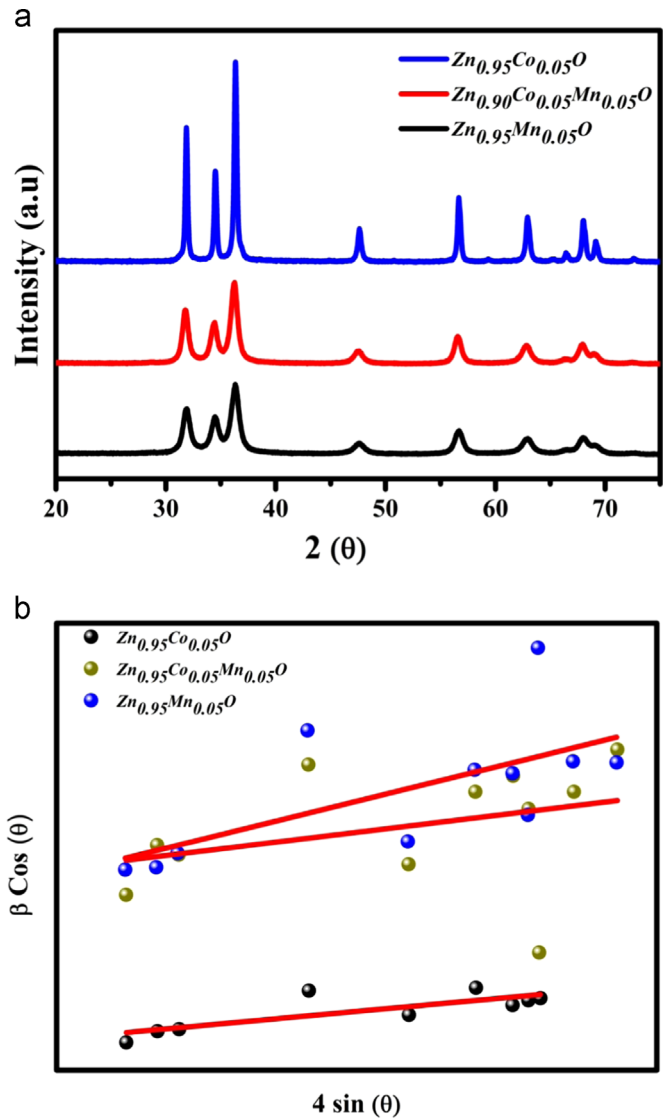


Fig. 1. (a) XRD pattern of ZC, ZM and ZCM samples; (b) W–H plot of ZC, ZM and ZCM samples.

by the doping of Mn in ZC sample.

From the XRD data, a few general parameters such as crystalline size, Lattice parameters, volumes and bond lengths were estimated as follows: The crystalline sizes were calculated by both the standard Scherrer's equation $\frac{0.94\lambda}{\beta \cos \theta}$ and Williamson–Hall (W–H) method. The lattice parameters such as a and c were calculated using a standard formula

$$\frac{1}{d_{hkl}^2} = \frac{4}{3} \left[\frac{h^2 + hk + k^2}{a^2} \right] + \frac{l^2}{c^2}.$$

Subsequently, the unit cell volume was also estimated [33]. Finally, the bond length between Zn and O has been calculated using the following relation

$$e = \sqrt{\left(\frac{a^2}{3} + \left(\frac{1}{2} - u \right)^2 c^2 \right)}$$

where u as a potential parameters of the structure [33]. Fig. 1 (b) shows the $4\sin \theta$ vs $\beta \cos \theta$ plots for calculating the lattice strain for the three samples. All these calculated parameters for the three samples were summarized in Table 1. From Table 1, it is observed that the crystalline sizes of all three samples estimated

Table 1

Calculated values of lattice parameters, lattice volume, bond length, c/a ratio, crystallite size, Lattice strain, optical band gap, magnetic retentivity and coercivity of the ZC, ZM and ZCM samples.

Name	$a=b\text{\AA}$	$c\text{\AA}$	Volume (\AA^3)	Bond length (nm)	c/a	u	Crystallite size (nm)		Strain W-H plot	Band gap (eV)		M_r (emu/g)	Coercivity (Oe)
							Scherrer	W-H plot		UV	PL		
$\text{Zn}_{0.95}\text{Co}_{0.05}\text{O}$	3.241	5.194	47.24	1.972	1.602	0.379	31	28	0.00164	3.317	3.3266	4.96×10^{-4}	62
$\text{Zn}_{0.95}\text{Co}_{0.05}\text{Mn}_{0.05}\text{O}$	3.242	5.20	47.34	1.974	1.603	0.379	12	12	0.00123	3.322	3.3266	0.0014	271
$\text{Zn}_{0.95}\text{Mn}_{0.05}\text{O}$	3.246	5.205	47.49	1.976	1.603	0.379	11	10	0.00331	3.322	3.335	0.00199	100

by both methods are almost in agreement with each other, and this confirms the reliability of these values.

Further, the structural factors such as lattice parameters and unit cell volumes of ZM and ZCM are higher than that of ZC. This is due to the fact that the substitution of larger ion Mn^{2+} (0.83 Å) in smaller ionic places like Co^{2+} (0.65 Å) and Zn^{2+} (0.74 Å). Hence, the doping of Mn in ZnO powders reduces the crystallite size. However, reduction in grain size occurs uniformly without any change in the c/a ratio, Zn–O bond length and crystalline structure.

3.2. Morphological studies

The surface morphological images of ZC, ZM and ZCM samples which have been carried out by HR-SEM are shown in Fig. 2(a–c) respectively. The ZC sample shows the coexistence of the sphere and hexagonal shape morphology, and it is in good agreement with earlier reports also [10]. However, the Mn doped samples ZM, ZCM appear grainy like morphology with an agglomeration of particles as shown in Fig. 2(b and c).

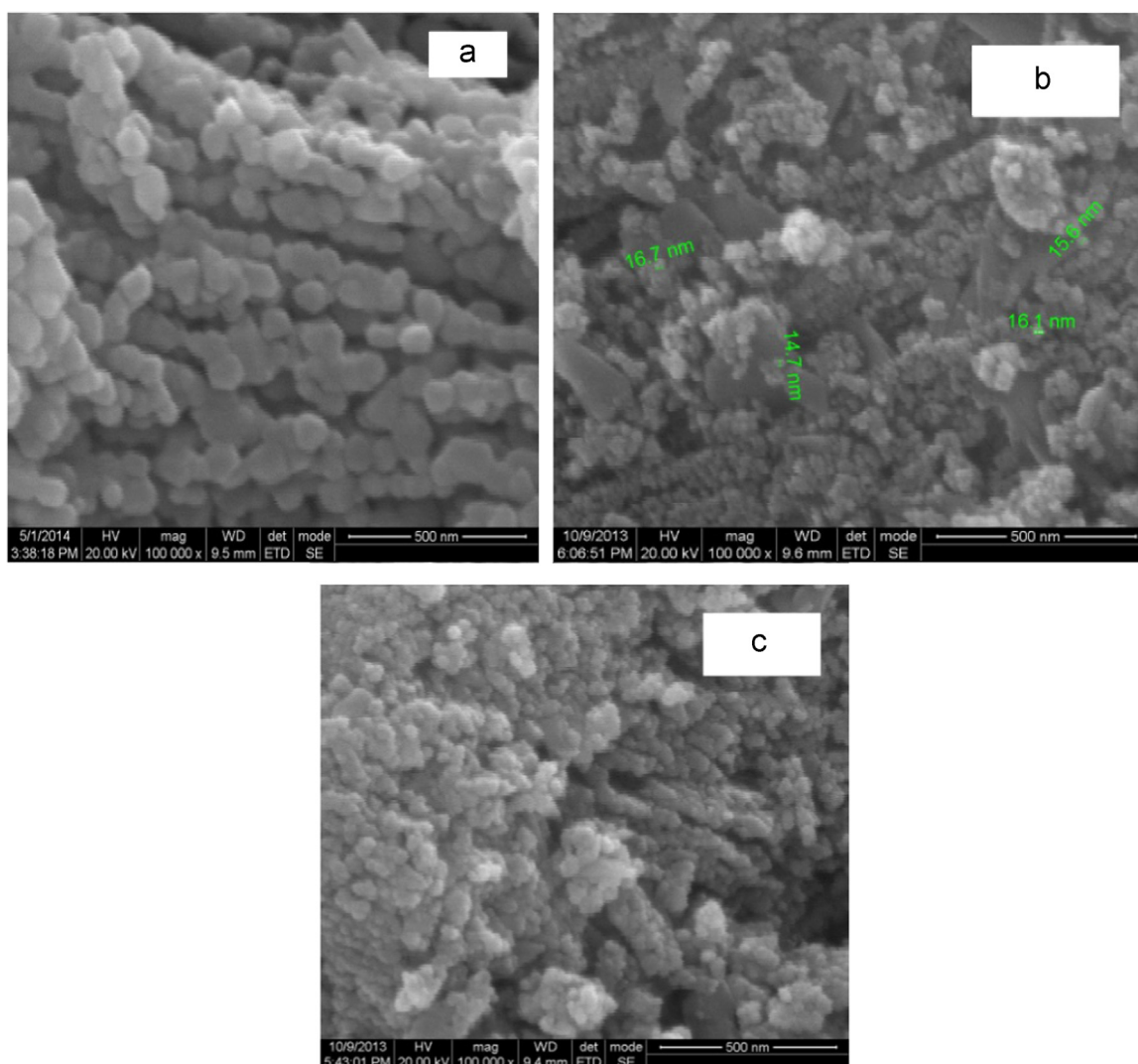


Fig. 2. HR-SEM image of (a) ZC, (b) ZM and (c) ZCM samples.

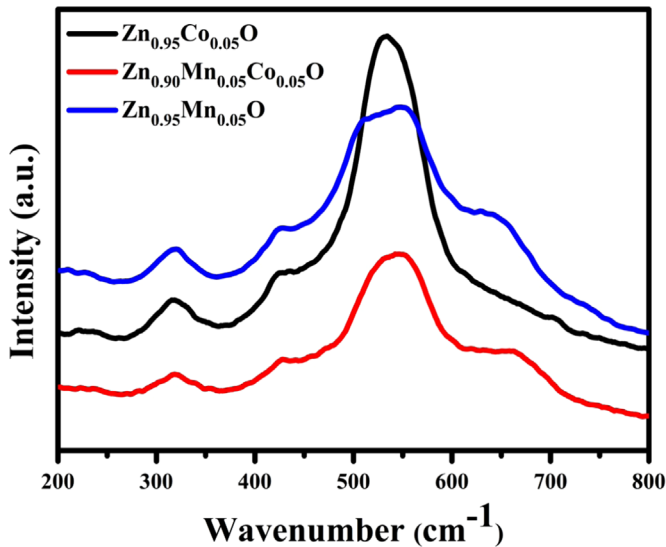


Fig. 3. Room temperature Raman spectra of the ZC, ZM and ZCM samples.

3.3. Raman studies

According to group theory, hexagonal Wurtzite structure with space group of $P6_3mc$ has different modes of vibrations, and these are represented by

$$A_1 + 2B_1 + E_1 + 2E_2$$

where A_1 and E_1 are polar modes, E_2 is non-polar mode and B_1 are a silent mode of Raman is scattering. Here, polar modes A_1 and E_1 possesses the transverse optical (TO) and longitudinal optical (LO) phonons respectively. Whereas, the non-polar E_2 mode comprises of both low and high frequencies. Hence, by analyzing the Raman scattering at room temperature for these samples may give a clear picture of the effect of doping and codoping on vibration modes.

Fig. 3 shows that Raman spectra of the ZC, ZM and ZCM samples at room temperature. For ZC sample, it shows non-polar vibrational modes of E_2^{low} , $E_2^{high-E_2^{low}}$ and E_2^{high} at 220 cm^{-1} , 330 cm^{-1} and 437 cm^{-1} respectively, and these values also are well in agreement with earlier reports [34,35]. On the other hand, for the Mn doped samples, the ZM and ZCM show an additional peak at 660 cm^{-1} . Since the doping effect of Mn^{2+} ions in ZC, introduces lattice defects, consequently shows a vibrational mode along Mn–O bonding [36–38]. Further, the strain introduced in the samples of ZM and ZCM is increased by the doping effect. Hence, the vibrational modes are shifted towards the lower wave number. Further, a broad peak around 540 cm^{-1} is also raised because of the lattice disorder and Zn interstitial defects and O related defects.

3.4. UV-DRS spectroscopy studies

In order to investigate the variation of optical bandgap with respect to doping, the optical absorption properties of these samples were measured through UV-absorption spectroscopic techniques. The optical absorption spectra for ZC, ZM and ZCM samples are shown in Fig. 4. From Fig. 4, the ZC and ZCM samples show a strong absorption peak at 360 nm and for the ZM sample the peak appears at slightly higher wavelength region. The optical band gap is estimated for all samples from the absorption edges and the results are tabulated in Table 1. The optical band gap also been estimated using Photoluminescence methods, which will be discussed in later sections. It is clear from Fig. 4 that the band gap of Mn doped samples such as ZM and ZCM samples is almost same, but smaller than standard undoped ZnO (3.327 eV). This

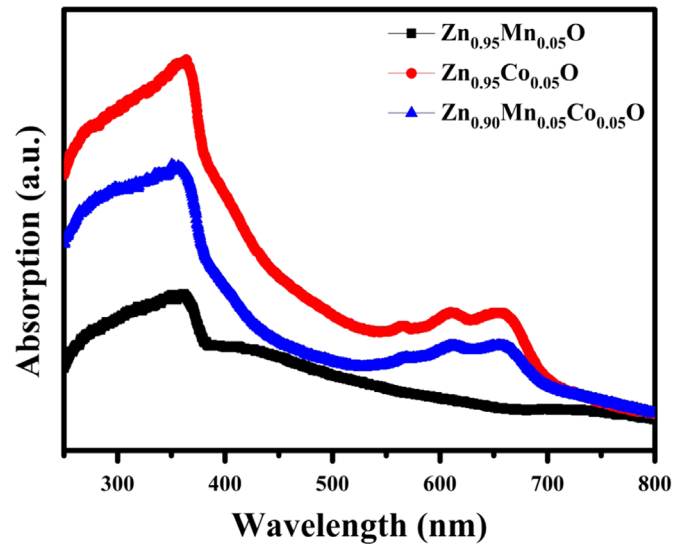


Fig. 4. UV-DRS spectra for ZC, ZM and ZCM samples.

trend is explained as follows: The localized electrons from d shell of dopant ions interact with sp electrons from the ZnO host lattice. Hence, an optical band gap for ZC, ZM and ZCM samples are decreased than pure ZnO. Moreover, a unique feature is observed only for Co doped samples, as shown in Fig. 4. The ZCM and ZC samples additionally show three absorption peaks at 569, 611 and 654 nm in the visible region. These additional peaks are coming out of the three different $d-d$ ($3d^7$) electronic transition in the high state of tetrahedral coordinates of Co^{2+} such as ${}^4A_2(F) \rightarrow {}^2A_1(G)$, ${}^4A_2(F) \rightarrow {}^4T_1(P)$ and ${}^4A_2(F) \rightarrow 2E(G)$ transitions respectively [39].

3.5. Photoluminescence studies

Photoluminescence (PL) is a suitable method for analyzing optical properties and lattice defects of metal oxide semiconductors. In this study, all the nanoparticles were excited using 325 nm wavelength. Fig. 5 shows the emission spectra for ZC, ZM and ZCM at room temperature. All the samples exhibit strong- and weak-emission spectra corresponding to UV- and visible-regions respectively. The strong emission in UV region originates from Near Band Edges (NBE) of the ZnO due to the recombination of free

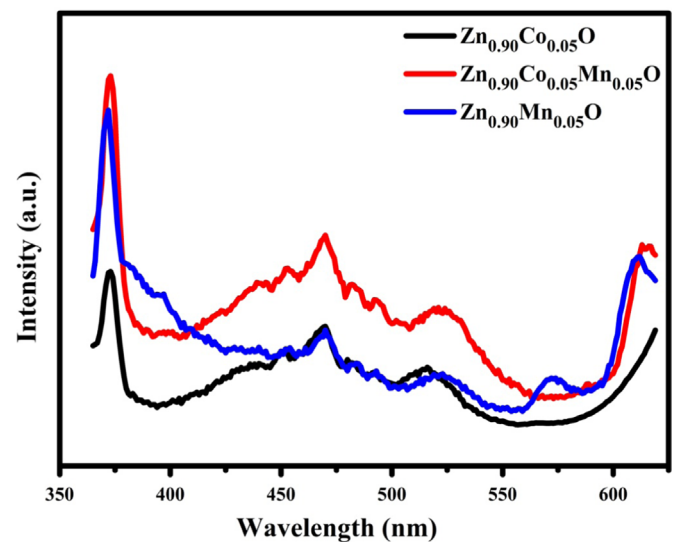


Fig. 5. Room temperature photoluminescence spectra of the ZC, ZM and ZCM samples.

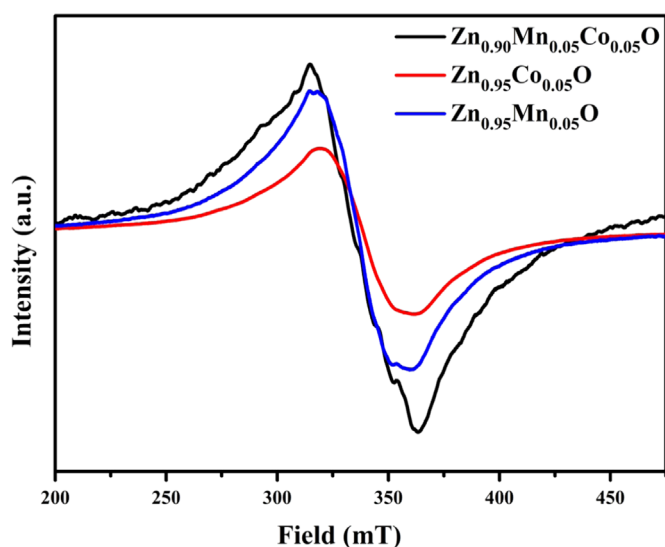


Fig. 6. Room temperature EPR spectrum for ZC, ZM and ZCM samples.

carriers through exciton-exciton process. The weak emission at visible region originates from lattice defects of metal oxide semiconductor nanoparticles. The optical band gap value was estimated from PL spectra for UV region emission, and it is given in the Table 1. These values will agree with UV-DRS spectroscopy values, and it confirms the consistency of values. Moreover, different emission peaks have raised in the visible region in the PL spectrum, such as blue, green and red emissions due to different types of lattice defects as given below: The blue (451 nm) and red (612 nm) emission appeared due to interstitial- and antisite-oxygen defects respectively, whereas the green region (470, 534 nm) emissions exist due to oxygen vacancy defects [4,7]. Additionally, green–yellow emission arises only in ZM and ZMC nanoparticles because of the incorporation of Mn^{2+} ions and Zn^{2+} site.

3.6. EPR studies

EPR spectroscopy technique was an effective tool for analyses the paramagnetic defects and incorporation of dopant ions in TM doped metal oxide semiconductor system. Fig. 6 represents the EPR signal for ZC, ZM and ZCM at room temperature. From Fig. 6, all the NPs were appeared broad signals, the broad signal was attributed to the ferromagnetic resonance (FMR). In EPR spectrum, ZC NP sample exhibits the smooth spectrum compared with ZM and ZCM. This is due to the rising of hyperfine spectrum by the incorporation of Mn^{2+} ions to ZnO host lattice [40]. The calculated g factor for the prepared NPs are 1.994, 2.007 and 2.021 for ZC, ZM and ZCM respectively. This factor value was associated with the presence of lattice defects such as Zn and Oxygen vacancies [41]. Hence, the presence of lattice defects in ZC, ZM, ZCM is confirmed by PL and EPR spectrum.

3.7. Magnetic properties

The magnetic properties of these samples are also studied through the magnetic field dependence of magnetization measurements at room temperature, and the corresponding results are shown in Fig. 7. All the three samples show the perfect ferromagnetic nature at room temperature. From Fig. 7, the magnetization retentivity (M_R) and coercivity are determined and reported in Table 1. The ZM sample has higher magnetization retentivity (M_R) compared to ZCM and ZC samples. Since, the interaction between Co–Co ions enhances AFM nature and hence ZCM gets lower M_R , whereas ZC sample gets lowest M_R among all.

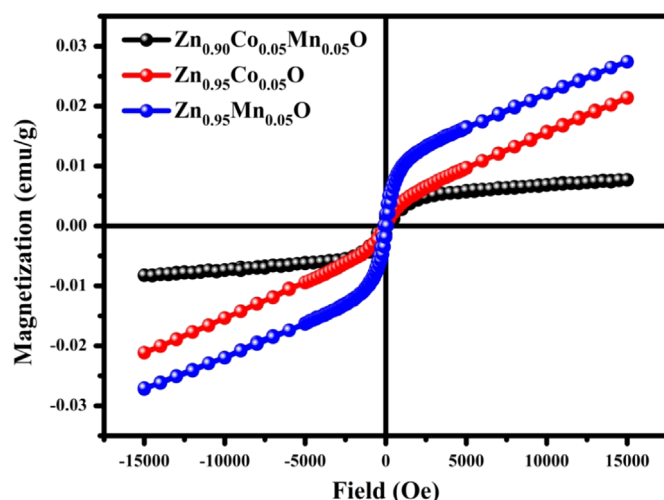


Fig. 7. Room temperature M–H curve of the ZC, ZM and ZCM samples.

On the other hand, the presence of Mn keeps the magnetic nature during the demagnetization cycle, and hence on doping of Mn increases the value of coercivity. Generally, metal oxide DMS materials exhibit the FM nature at room temperature and above. However, the origin of this Ferromagnetic nature is still unclear. Dopant related secondary phase (CoO , Co_2O_4 and Mn_2O_3), dopant metal clusters [42] and/or spinel phase ($ZnMn_2O_4$, $ZnCo_2O_4$) [43] were drastically induced the ferromagnetic behavior. Earlier, Jayakumar et al. reported that the appearance of ferromagnetism in Mn doped ZnO polycrystalline is raised by secondary peaks [5]. Kumar et al. reported ferromagnetism in Fe doped ZnO material at room temperature due to the charge (hole) mediation [6]. According to RKKY theory, the exchange interaction between localized dopant electrons and sp electron of host material are responsible for the RTFM behavior in DMS materials [9,31]. Coey et al. proposed F-center exchange interaction between TM–O–TM leads to RTFM in Co doped ZnO system [44]. Further, the oxygen related defects also play a vital role in RTFM of DMS materials, both in undoped and/or some transition metals (Ni, Co, Mn, Fe and Cu) doped ZnO nanoparticles [4,7,10–12]. However, the non-magnetic mono-valent ions like Cu^+ , Na^+ ions codoped ZnO: Co powders were displayed ferromagnetism due to Zn interstitial defects [45]. In our earlier work, the undoped and non-magnetic 1st group elements doped ZnO nanoparticles displayed ferromagnetism ascribed to the presence of Zn interstitial and oxygen vacancy complex defects [46]. Undoped ZnO and non-magnetic ions doped ZnO appeared RTFM and this type of magnetism was claimed by d^0 ferromagnetism [47,48]. Strumal et al. reported the ferromagnetic behavior in ZnO was led to grain boundary networks [49,50]. In the present work, as discussed above, Raman, PL and EPR spectroscopy studies suggested the presence of Zn interstitial and single ionized oxygen defects. Moreover, the introduction of Mn ions in ZnO lattice decreases their grain size and simultaneously grain boundary region gets increased. Hence, the coercivity of ZM, ZCM was higher than ZC due to the grain boundary networks. Above all, these reasons, it is evidenced that ZC, ZM and ZCM nanoparticles exhibit RTFM behavior.

4. Conclusions

In conclusion, the single phase $Zn_{0.95}Co_{0.05}O$, $Zn_{0.95}Mn_{0.05}O$ and $Zn_{0.90}Co_{0.05}Mn_{0.05}O$ DMS nanoparticles have been successfully synthesized by co-precipitation method. The doping of Mn reduces the grain sizes of systems from 31 nm to 11 nm, subsequently the

lattice strain also enhanced. The EPR spectrum of the samples, exhibits a broad resonance signal centered at 1.994, 2.007 and 2.021 for ZC, ZM and ZCM respectively. The optical band gap decreases than standard pure ZnO due to grain confinement effect. The appearance of broad peaks in Raman spectra and visible region emissions in PL spectra of all samples have confirmed the presence of lattice defects. These defects lead to the RTFM behavior in all the samples. Moreover, the coercivity and the retentivity of ZM and ZCM was higher than ZC due to the grain boundary networks.

Acknowledgments

Author V.Pazhanivelu thanks to UGC, Govt of India [Project No: 40-444/2011 (SR)] for research fellowship and R.Thiyagarajan and Yongsheng Zhao acknowledge NSAF (Grant No: U1530402) for fellowship.

References

- [1] U. Ozgur, Y.I. Alivou, C. Liu, A. Teke, M.A. Reshchikov, S. Dogan, V. Vrutin, S. J. Cho, H. Morkoc, *Appl. Phys. Lett.* 98 (2005) 041301.
- [2] T. Dietl, H. Ohno, F. Matasakura, J. Cibert, D. Ferrand, *Science* 287 (2000) 1019.
- [3] Hui Liu, Xiao Zhang, Luyan Li, Y.X. Wang, K.H. Gao, Z.Q. Li, R.K. Zheng, S. P. Ringer, Bei Zhang, X.X. Zhang, *Appl. Phys. Lett.* 91 (2007) 072511.
- [4] Ting Guo, Yujung Zhang, Yidong Luo, Ce-Wen Nan, Yuan-Hua Lin, *J. Appl. Phys.* 112 (2012) 083916.
- [5] O.D. Jayakumar, H.G. Salunke, R.M. Kadam, M. Mohapatra, G. Yaswant, S. K. Kulshreshtha, *Nanotechnology* 17 (2006) 1278.
- [6] S. Kumar, Y.J. Kim, B.H. Koo, S.K. Sharma, J.M. Vargas, M. Knobel, S. Gautam, K. H. Chae, D.K. Kim, Y.K. Kim, C.G. Lee, *J. Appl. Phys.* 105 (2009) 07C520.
- [7] Gunjan Srinet, Ravindra Kumar, Vivek Sajal, *J. Appl. Phys.* 114 (2013) 033912.
- [8] R. Boubekri, Z. Beji, K. Elkabous, F. Herbst, G. Viau, S. Ammar, F. Fiévet, H.J. Von Bardeleben, A. Mauger, *J. Chem. mater.* 21 (2009) 843.
- [9] Y.K. Lakshmi, K. Srinivas, B. Sreedhar, M.M. Raja, M. Vithal, P.V. Reddy, *J. Mater. Chem. Phys.* 113 (2009) 749.
- [10] V. Pazhanivelu, A. Paul Blessington Selvadurai, R. Murugaraj, *J. Supercond. Novel Magn.* 28 (2015) 2575.
- [11] K. Samanta, K.P. Bhattacharya, R.S. Katiyar, *J. Appl. Phys.* 105 (2009) 113929.
- [12] Hao Gu, Yinzhong Jiang, Yongbing Xu, Mi Yan, *J. Appl. Phys.* 98 (2011) 012502.
- [13] R. Laiho, I. Ojala, L. Vlasenko, *J. Appl. Phys.* 108 (2010) 053915.
- [14] P. Photongkam, Y.B. Zhang, M.H.N. Assadi, S. Li, D. Yu, M. Ionescu, A.V. Pan, *J. Appl. Phys.* 107 (2010) 033909.
- [15] Min Zhong, Shiwei Wang, Ying Li, Yemin Hu, Mingyuan Zhu, Hongmin Jin, Yibing Li, Haimin Zhang, Huijun Zhao, *J. Ceram. Int.* 41 (2015) 451.
- [16] Kongping Wu, Shulin Gu, Kun Tang, Shunming Zhu, Jiandong Ye, Rong Zhang, Youdou Zheng, *Thin. Solid Films* 519 (2011) 2499.
- [17] H.B. Ruan, L. Fang, G.P. Qin, T.Y. Yang, W.J. Li, F. Wu, M. Saleem, C.Y. Kong, *Solid State Commun.* 152 (2012) 1625.
- [18] Kongping Wu, Shulin Gu, Kun Tang, Jiandong Ye, Shunming Zhu, Mengran Zhou, Yourui Huang, Mingxiang Xu, Rong Zhang, Youdou Zheng, *J. Magn. Mater.* 324 (2012) 1649.
- [19] L.Q. Zhang, Z.Z. Ye, B. Lua, J.G. Lu, J.Y. Huang, Y.Z. Zhang, Z. Xie, *Solid State Commun.* 155 (2013) 16.
- [20] C.W. Zou, H.J. Wang, M.L. Yi, M. Li, C.S. Liu, L.P. Guo, D.J. Fu, T.W. Kang, *Appl. Surf. Sci.* 256 (2010) 2453.
- [21] C.W. Zou, L.X. Shao, L.P. Guo, D.J. Fu, T.W. Kang, *J. Cryst. Growth* 331 (2011) 44.
- [22] Jiu-Ping Fan, Feng-Xian Jiang, Xiu-Fang Qin, Xiao-Hong Xu, *Physica B* 407 (2012) 2215.
- [23] R. Thankalekshmi, A.C. Rastogi, *J. Anal. Appl. Pyrolysis* 107 (2014) 183.
- [24] Jiuping Fan, Fengxian Jiang, Zhiyong Quan, Xiufang Qing, Xiaohong Xu, *Mater. Res. Bull.* 47 (2012) 3344.
- [25] N. Rajamanickam, R.N. Mariammal, S. Rajashabala, K. Ramachandran, *J. Alloy. Compd.* 614 (2014) 151.
- [26] S.K. Neogi, S. Chattopadhyay, R. Karmakar, Aritra Banerjee, S. Bandyopadhyay, A. Banerjee, *J. Alloy. Compd.* 573 (2013) 76.
- [27] J. Das, D.K. Mishra, V.V. Srinivasu, D.R. Sahu, B.K. Roul, *J. Magn. Mater.* 382 (2015) 111.
- [28] Min Zhong, Ying Li, Yemin Hu, Mingyuan Zhu, Wenxian Li, Hongmin Jin, Shiwei Wang, Yibing Li, Huijun Zhao, *J. Alloy. Compd.* (2015).
- [29] Kai-Cheng Zhang, Yong-Feng Li, Yong Liu, Yan Zhu, *Physica B* 451 (2014) 43.
- [30] L.B. Duan, G.H. Rao, Y.C. Wang, J. Yu, T. Wang, *J. Appl. Phys.* 104 (2008) 013909.
- [31] Hengda Li, Xinzhong Liu, Zhigong Zheng, *J. Magn. Mater.* 372 (2014) 37.
- [32] Sabiu Said Abdullahi, Yuksel Köseoglu, Sadik Güner, Sinan Kazan, Bayram Kocaman, Chifu E. Ndikilar, *Superlattice Microstruct.* 83 (2015) 342.
- [33] S. Sivaselvan, S. Muthukumar, M. Ashokkumar, *Opt. Mater.* 36 (2014) 797.
- [34] Q.Q. Gao, Q.X. Yu, K. Yuan, X.N. Fu, B. Chen, C.X. Zhu, H. Zhu, *Appl. Surf. Sci.* 264 (2013) 7.
- [35] Gugu H. Mhlongo, David E. Motaung, Steven S. Nkosi, H.C. Swart, Gerald F. Malgas, Kenneth T. Hillie, Bonex W. Mwakikunga, *Appl. Surf. Sci.* 293 (2014) 62.
- [36] C.X. Xu, X.W. Suna, Z.L. Dong, S.T. Tan, Y.P. Cui, B.P. Wang, *J. Appl. Phys.* 98b (2005) 113513.
- [37] H.S. Kim, P.C. Stair, *J. Phys. Chem. B* 108 (2004) 17019.
- [38] L.W. Yang, X.L. Wu, G.S. Huang, T. Qiu, Y.M. Yang, *J. Appl. Phys.* 97 (2005) 014308.
- [39] Hongjing Hao, Mei Qin, Ping Li, *J. Alloy. Compd.* 515 (2012) 143.
- [40] D. Toloman, A. Mesaros, A. Popa, O. Raita, T.D. Silipas, B.S. Vasile, O. Pana, L. M. Giurgiu, *J. Alloy. Compd.* 551 (2013) 502.
- [41] D.E. Motaung, P.R. Makgwane, S.S. Ray, *Mater. Lett.* 139 (2015) 475.
- [42] J.E. Ramos, M. Montero-Munoz, J.A.H. Coaquira, J.E. Rodriguez-Paez, *J. Appl. Phys.* 115 (2014) 17E123.
- [43] K. Samanta, P. Bhattacharya, R.S. Katiyar, *Phys. Rev. B* 73 (2006) 245213.
- [44] J.M.D. Coey, A. Douvalis, C. Fitzgerald, M. Venkatesan, *Appl. Phys. Lett.* 84 (2004) 1332.
- [45] Yanyan Wei, Denglu Hou, Shuang Qiao, Congmian Zhen, Guide Tang, *Physica B* 404 (2009) 2486.
- [46] V. Pazhanivelu, A. Paul Blessington Selvadurai, R. Murugaraj, *Mater. Lett.* 151 (2015) 112.
- [47] J.M.D. Coey, M. Venkatesan, P. Stamenov, C.B. Fitzgerald, L.S. Dorneles, *Phys. Rev. B* 72 (2005) 024450.
- [48] C.D. Pemmaraju, S. Sanvito, *Phys. Rev. Lett.* 94 (2005) 217205.
- [49] B.B. Straumal, A.A. Mazilkin, S.G. Protasova, P.B. Straumal, A.A. Myatiev, G. Schütz, E. Goering, B. Baretzky, *Phys. Met. Metallogr.* 113 (2012) 1244.
- [50] B.B. Straumal, A.A. Mazilkin, S.G. Protasova, A.A. Myatiev, P.B. Straumal, E. Goering, B. Baretzky, *Thin. Solid Films* 520 (2011) 1192.